Novel Preclinical Human Salivary Gland Cancer Models Established Using Organoid Culture And Patient-Derived Xenografting

Yoshihiro Aizawa
Yokohama City University
Kentaro Takada
Yokohama City University
Jun Aoyama
Yokohama City University
Daisuke Sano (dsano@yokohama-cu.ac.jp)
Yokohama City University https://orcid.org/0000-0002-7686-4724
Shoji Yamanaka
Yokohama City University Hospital
Masahide Seki
Graduate School of Frontier Sciences, The University of Tokyo https://orcid.org/0000-0001-6091-8698
Yuta Kuze
The University of Tokyo
Jordan Ramilowski
Yokohama City University https://orcid.org/0000-0002-3156-6416
Ryo Okuda
Roche Institute for Translational Bioengineering
Yasuharu Ueno
Center for Stem Cell Biology and Regenerative Medicine
Yusuke Nojima
Yokohama City University
Yoshiaki Inayama
Yokohama City University Medical Center
Hiromitsu Hatakeyama
Yokohama City University Medical Center
Takashi Hatano
Yokohama City University
Hideaki Takahashi
Yokohama City University
Goshi Nishimura
Yokohama City University
Satoshi Fujii
Yokohama City University Graduate School of Medicine

Yutaka Suzuki
University of Tokyo https://orcid.org/0000-0003-4852-1879
Hideki Taniguchi
The Institute of Medical Science, the University of Tokyo
Nobuhiko Oridate
Yokohama City University

Article

Keywords: histological subtypes, organoid, pathogenesis, PDX

Posted Date: September 3rd, 2021

DOI: https://doi.org/10.21203/rs.3.rs-779030/v1

Abstract

Salivary gland carcinoma (SGC) has poor prognosis depending on the histological subtype. However, due to the scarcity of preclinical experimental models, its pathogenesis remains largely unknown, hampering the development of new treatment modalities for patients with these malignancies. Here, we first report the establishment of a large collection of human SGC experimental models for multiple histological subtypes using patient-derived xenograft (PDX) and organoid culture techniques with our previously optimized method. Additionally, we successfully generated organoids by culturing established PDXs (PDX-derived organoids). Through passaging, each pre-clinical model was confirmed to maintain the pathological characteristics of the original tumor and the genetic traits of corresponding histological subtypes. Finally, we confirmed that these organoids were available for pharmacologic studies. Thus, our comprehensive models of SGC could be a powerful resource for the development of novel therapeutic agents and investigating the pathogenesis of these malignancies.

Introduction

Salivary gland carcinomas (SGCs) are uncommon malignancies, representing approximately 0.3% of all cancers, with the estimated world annual incidence of 0.05 to 2 per 100,000 population[1,2]. These malignancies exhibit considerable pathologic, biological, and clinical diversity. Currently, there are 24 histological subtypes[3]; therefore, accurate preoperative diagnosis of these diseases has become quite difficult in clinical practice[4–6]. Among the many histological subtypes, salivary duct carcinoma (SDC) is highly malignant with a high rate of distant metastatic recurrence and a 5-year survival rate of only 40%[7,8]. Adenoid cystic carcinoma (ACC) is one of the most common histological subtypes of SGCs, characterized by high rate of perineural invasion, local recurrence, and delayed onset of distant metastases[9,10]. The prognosis of mucoepidermoid carcinoma (MEC), another common type of SGCs, is highly dependent on the pathological grade, with a 5-year survival rate of 22.5–52% in high-grade cases, and a majority of patients die from distant metastasis rather than local recurrence[11–13]. Thus, patients diagnosed with some aggressive histological subtypes of SGCs represent poor prognosis.

Despite this background, the disease pathogenesis of SGCs remains unclear[14,15], except in cases of tumor-specific recurrent chromosomal translocations that result in the formation of fusion genes, such as CRTC1 [MECT1]-MAML2 identified in MEC[16] or MYB-NFIB in ACC[17]. The lack of *in vitro* and *in vivo* SGC models that can effectively recapitulate the diversity of human SGC has hampered the understanding of disease progression.

Recently, patient-derived xenograft (PDX) and organoid cultures have emerged as useful preclinical tools to overcome problems in traditional two-dimensional culture by mimicking traits and heterogeneity of the original tumor[18–20]; these technologies have the potential to be a stepping stones to personalized medicine[19,21,22]. We previously reported the successful establishment of human ACC-derived-organoid lines, short-term organoid lines from ACC PDX, and organoids-transplanted animal model of ACC, reproducing the histological characteristics of original tumor, and showed the significance of our model for preclinical drug screening evaluation[23]. Here, we established comprehensive preclinical models of SGCs, including SDC, MEC, and myoepithelial carcinoma (MYEC), using organoid culture and patient-derived xenografting. Additionally, we genetically characterized these novel preclinical models of SGC using RNA-seq analysis, next-generation sequencing, and demonstrated *in vitro* drug sensitivity test.

Methods

Human Specimens. We obtained 40 fresh SGC tumor tissues from patients undergoing surgical resection at Yokohama City University Hospital or Yokohama City University Medical Center (Yokohama, Japan) and stored them in culture medium on ice until further use (< 12 h). The pathological diagnosis for each case was confirmed by independent pathologists after sample collection. We obtained written informed consent from all patients prior to surgery. The current study was approved by the ethical committees of the Institutional Review Boards of the Yokohama City University (approval IDs: A171130010) and was conducted in accordance with the Declaration of Helsinki.

Patient-derived xenografts (PDX). PDX were established by subcutaneous implantation of fresh minced tumors into NOD Cg-Prkdc^{scid} Il2rg^{tm1Wjl} (NSG) mice as previously described[23]. All mice were dissected to visually examine for metastases in lung, liver, and abdominal cavity. All mice were maintained and handled in accordance with the procedures approved by the Institutional Animal Care Use Committee at Yokohama City University, School of Medicine (Yokohama, Japan).

Organoid culture. Organoid cultures from patient specimens and PDX were performed as previously described[23]. The tissue, cut into 2–4 mm pieces, was enzymatically digested with Liberase TM Research Grade (Sigma Aldrich, St. Louis, MO, USA) and Hyaluronidase (Sigma Aldrich) for 30–60 min at 37°C. Processed tissue was passed through a 70 μm cell strainer (Corning Incorporated, Corning, NY, USA) to eliminate macroscopic pieces. The isolated cells were suspended in complete media (AdDMEM/F12 medium supplemented with HEPES [Invitrogen, Carlsbad, CA, USA], Glutamax [Invitrogen], penicillin/streptomycin [Invitrogen], B27 [Invitrogen], 1 mg/m Primocin [InvivoGen, San Diego, CA, USA], 1 mM N-acetyl-l-cysteine [Sigma-Aldrich], 500 ng/mL Wnt3a [R&D systems, Emeryville, CA, USA], 0.1 μg/mL R-spondin1 [Peprotech, Rocky Hill, NJ, USA], 0.1 μg/mL Noggin [Peprotech], 50 ng/mL epidermal growth factor [Sigma-Aldrich], 100 ng/mL fibroblast growth factor 10 [Peprotech], 10 mM Nicotinamide [Sigma-Aldrich], 0.1 μM A83-01 [Sigma-Aldrich] and 1 μM Dexamethasone [Sigma-Aldrich]) and seeded on growth-factor-reduced (GFR) Matrigel (Corning Incorporated) coated plate, pre-prepared as a lower layer. After incubation for 16–24 hours, the media was removed and the organoids formed on the lower layer were covered with additional GFR Matrigel as an upper layer. The complete media was added after the formation of solid coating, and the media was changed every 2–3 days.

For passaging, the Matrigel containing organoids was collected from the plate, and digested with TrypLE Express Enzyme (Thermo Fisher Scientific, Waltham, MA, USA). Isolated organoids were suspended in DMEM/F12 media and physically crushed into smaller cell clumps by pipetting. Cells were centrifuged, re-suspended in complete media with 10 μM ROCK inhibitor (Y-27632, Sigma), and then embedded in GRF Matrigel as described above. Organoids were passaged at a 1:2 to 1:1.5 dilution ratio every 2–3 weeks. To prepare frozen stocks, organoids were isolated and suspended in CELLBANKER 1 (TAKARA-BIO, Kusatsu, Shiga, Japan) and stored in − 80°C freezer or liquid nitrogen. Stocks have been successfully recovered for up to at least 6 months after freezing. STR analysis was performed at BEX. CO., LTD. (Tokyo, Japan) to authenticate the identity of organoids and corresponding patient tissue. To check the contamination of mouse cells, we performed PCR of animal species-specific mitochondrial DNA sequences[42] using the primers listed in Supplementary Table S3. Organoids were routinely tested for Mycoplasma using e-Myco VALiD Mycoplasma PCR Detection Kit (iNtRON Biotechnology, Seoul, Korea).

Orthotopic transplantation. For orthotopic transplantation of SGC organoids, organoids were injected into the submandibular gland and subcutaneously in NSG mice as previously described[23]. The submandibular gland was injected with 0.5×10^5 to 1×10^6 cells suspended in a mixture of DMEM/F12 media and Matrigel, and the subcutaneous area was similarly injected with 1 to 2×10^6 cells. Orthotopic xenograft volumes were measured weekly. Xenografts were harvested when the tumor diameter reached > 1 cm or 6 months after implantation and fixed for 24 h in 10% formalin.

IHC analysis. Fresh PDXs and orthotopic xenografts were fixed in 10% formalin for 24 h and then embedded in paraffin following standard histological procedures. Organoids were isolated by digesting Matrigel using dispase (Sigma) for 30 min at 37°C and embedded into a gel using iPGell (GenoStaff, Tokyo, Japan) according to the manufacturer's protocol. Next, the organoids were fixed in 10% formalin for 24 h and paraffin-embedded. Haematoxylin–eosin staining and IHC were performed using standard protocols on 5-μm-thick paraffin sections. The following antibodies were used for IHC: human-Androgen Receptor (AR441, Dako, Carpinteria, CA, USA) 1:500, pan keratin AE1/AE3/PCK26 (Roche, Basel, Switzerland) 1:1, HER2 (4B5, Roche) 1:1, alpha-smooth muscle actin (S131, Leica Biosystems, Buffalo Grove, IL, USA) 1:1, p63 (4A4, Biocare medical, Concord, CA, USA) 1:200, S-100 (Roche) 1:1000, and GCDFP15 (D6, Biocare medical) 1:400. Images were acquired using an OLYMPUS BX41 microscope.

DNA/RNA extraction. Organoids were extracted from Matrigel using TrypLe. Total RNA was extracted from organoids using TRIzol (Thermo Fisher), followed by isolation and precipitation in chloroform and 70% ethanol, and then purified via column-based separation using the RNeasy Mini Kit (QIAGEN, Valencia, CA). DNA was extracted from organoids using DNA mini kit (QIAGEN) according to the manufacturer's protocol. PDX tissues harvested from mice, as well as tissue fragments of primary salivary gland tumor, were physically homogenized using a plastic homogenizer vessel. RNA and DNA extraction from these homogenized tissues were processed similarly as described above.

RNA-sEq. RNA sequencing was performed at the Laboratory of Systems Genomics, Department of Computational Biology and Medical Sciences, at the University of Tokyo (Chiba, Japan). RNA quality and quantity were measured with an Agilent Bioanalyzer 2100. Libraries for sequencing were constructed using TruSeq Stranded mRNA (Illumina, San Diego, CA, USA)) according to the manufacturer's protocol, followed by sequencing on an Illumina NovaSeq6000 platform to generate 70 million paired-end reads of 150 bases. The RNA-seq data are available at the DNA Data Bank of Japan Sequence Read Archive (DRA) under the accession number DRA011243.

Gene expression analysis. RNA-seq reads were quality checked and adapter trimmed using fastp (v0.20.1)[43]. Since RNA-seq reads derived from PDX tumors and PDX-derived organoids both essentially contain mouse reads, we distinguished the trimmed reads into those of humans (GRCh38/hg38) or mice (GRCm38/mm10) using xenome (v1.0.0)[44]. Only human reads were used for subsequent processing. Mouse reads and indistinguishable reads were discarded. To ensure consistency in process sampling, samples that do not contain intrinsic mouse reads, such as primary organoids, were processed in the same manner as described above. The human reads were aligned to human genome reference sequence (GRCh38/hg38) using STAR (v2.7.5c)[45] and counted for each gene using featureCounts (v2.0.1)[46]. For a heatmap, hierarchical clustering analysis with complete linkage and Euclidean distance, and correlation analysis, the raw read counts per gene with at least an average of 5 counts were TMM normalized using edgeR (v3.30.3)[47] and log2-transformed. The heatmap and clustering analysis were visualized with the top 2000 variable genes using R package "pheatmap." The Pearson's correlation coefficients

were for calculated for all genes. For a principal component analysis (PCA), we combined our samples with RNA-seq datasets of multiple salivary gland cancers downloaded from public databases. SRP067524 (including 42 samples of ACC and 5 samples of normal salivary gland), SRP067827 (including 3 samples of acinic cell carcinoma), SRP096726 (including 16 samples of SDC), and SRP109264 (including 40 samples of MEC) were downloaded from the NCBI Sequence Read Archive. The raw read counts per gene for all samples were calculated as described above and were normalized for library size by converting to CPM (counts per million) using edgeR[47]. The R package “sva” (v3.36.0)[48] was applied to adjust for batch effects, along with information of histological subtype of each sample. PCA was performed using the “prcomp” function in R.

Variant calling. SNP discovery and filtering from RNA-seq data were performed using HaplotypeCaller under standard parameters according to GATK[24] (v4.1.8) Best Practices (https://github.com/gatk-workflows/gatk3-4-rnaseq-germline-snps-indels). Additionally, SNPs with a depth < 25 and an allele frequency < 0.2 were excluded. The functional effects of the mutations were predicted using SnpEff (v5.0)[49], and SNPs with "high" or "moderate" functional importance were retained. To visualize representative genes that are mutated in salivary gland tumors in COSMIC[25], the vcf format data was converted to maf format data using ANNOVAR[50] and annovarToMAF under standard parameters, and the "waterfall" function of R package GenVisR (v1.20.0) [51] was applied.

Detection of fusion genes. Candidate fusion genes were explored from RNA-seq data using STAR-Fusion (v1.6.0)[45], FusionCatcher (v1.20)[52], and a combination of kallisto (v0.46.2)[53] and pizzly (v0.37.3)[54]. The detected candidate fusion genes were cross-referenced to ChimerDB4.0[55], and those reported in salivary gland carcinoma were extracted and validated by RT-PCR. RT-PCR was performed as previously described[50] using PrimeScript 1st strand cDNA Synthesis Kit (TAKARA-BIO), and RT-PCR products were subjected to Sanger sequencing at Macrogen Japan (Tokyo, Japan). All primers used are listed in Supplementary Table S3.

Drug sensitivity test. Drug sensitivity test was performed as previously described[23] using CellTiter-Glo 3D (Promega). All available organoids were evaluated for sensitivity to cisplatin (3.12–800 μM range), docetaxel (0.24 nM to 4.0 μM range), and fluorouracil (0.39 μM to 6.4 mM range). Additionally, organoids derived from SDC were evaluated for sensitivity to trastuzumab (0.3 μM to 5 mM range), an anti-HER2 antibody agent. A253 cell line, as a control group, was evaluated for sensitivity to cisplatin, docetaxel, fluorouracil, and trastuzumab. Each test was repeated at least thrice. The dose-response curve was obtained as the output, and the IC50 was calculated using the four parameter logistic equation and the R package “drc” (v3.0.1)[56].

Statistical analysis. The association between the establishment rate of each experimental model and the clinical information of the patients was tested using Fisher's exact ratio test and Student’s *t*-test in the open-source R Statistical Computing software (http://www.r-project.org/). Statistical significance was set at $P < 0.05$.

Results

Human SGC organoid culture and PDX. We established a series of human SGC-derived organoid lines and PDX models using human SGC tumor section (Table 1) by optimizing our existing protocol for human-ACC derived organoid and PDX models[23]. Comprehensive clinical information of the patients involved in the present study is shown in Supplementary Table S1. As the overview of our examinations (Fig. 1), we aimed to establish both human SGC-derived organoid and PDX if enough tumor specimens were secured. Additionally, we sought to generate *ex vivo* organoid culture of cells isolated from the established PDX tumors. To date, human SGC-derived

organoids have only been successfully generated using SDC (YCU-SDC-14, YCU-SDC-20, and YCU-SDC-32) and MEC (YCU-MEC-24) specimens in this study. PDXs have been also established using SDC (YCU-SDC-14 PDX, YCU-SDC-20 PDX), MEC (YCU-MEC-24 PDX), and MYEC (YCU-MYEC-16 PDX). Additionally, PDX-derived organoids (YCU-SDC-14X, YCU-SDC-20X, and YCU-MEC-24X) have been successfully generated using YCU-SDC-14 PDX, YCU-SDC-20 PDX, and YCU-MEC-24PDX, respectively. Each generated organoid was confirmed to be a genetic match of the original tumor by short tandem repeat (STR) profiling. Thus, YCU-SDC-14, YCU-SDC-20, and YCU-MEC-24 specimens were able to generate human tumor-derived organoid lines, PDX models, and PDX-derived organoid lines (Table 1).

Table 1. Summary of patient-derived xenograft (PDX) and organoid lines, corresponding clinical data. The clinical stage of the tumor was at the time of the first treatment, not during the entire clinical course of the patient. See Supplemental Table 1 for information on all patients from whom the specimens were collected

Name	Sex	Age	Pathological diagnosis	Primary site	TNM stage (7^{th} edition)			Last passage		
					T	N	M	PDX	Primary organoid	PDX-derived organoid
YCU-ACC-1	F	48	Adenoid cystic carcinoma	Nasal cavity	4a	0	0	10[a]	2[b]	4[b]
YCU-ACC-4	M	67	Adenoid cystic carcinoma	Sublingual gland	4a	2c	1	10[a]	9[b]	9[b]
YCU-SDC-14	M	51	Salivary duct carcinoma	Submandibular gland	3	3b	0	8[a]	55[a]	35[a]
YCU-MYEC-16	M	73	Carcinoma ex pleomorphic adenoma (Myoepithelial carcinoma)	Parotid gland	2	0	0	7[a]	1[b]	5[b]
YCU-SDC-20	M	71	Salivary duct carcinoma	Parotid gland	4a	1	0	9[a]	52[a]	40[a]
YCU-MEC-24	F	55	Mucoepidermoid carcinoma	Oral floor	4a	2b	0	5[a]	25[b]	35[a]
YCU-SDC-32	M	72	Carcinoma ex pleomorphic adenoma (Salivary duct carcinoma)	Parotid gland	2	0	0	0[b]	36[a]	Not available

a As of March 2021.

b Not being actively passaged at the time of publication.

Our SGC PDX models were capable of up to 10 passages. YCU-SDC-14 PDX model often developed liver metastases after the first passage (Supplementary Fig. S2a). Human SGC-derived organoids aggregated on Matrigel and generated cystic formation when maintained in culture with a passaging ratio of 1:1.5 to 1:2 approximately every 14 days with up to 55 passages (Fig. 2 and Supplementary Fig. S1). These organoids and PDXs showed a wide spectrum of proliferative activity, e.g. YCU-SDC-32 were able to passage more than 35 times as human tumor-derived organoid; however, the growth of PDX was slow, not yielding sufficient quantities for passaging of PDX or PDX-derived organoid culture.

Overall, we found that PDXs were established from 6 (20.7%) of the 29 patients, and human SGC-derived organoids were established from 4 (11.4%) of the 35 patients (Supplementary Table S1). Additionally, PDX-derived organoids were generated from 3 (50.0%) of the 6 established PDXs (Supplementary Table S1). We did not observe any correlation between the establishment success rate for each model and clinical characteristics (data not shown). Our models were successfully recovered after the long-term preservation for at least 6 months in −80°C.

PDXs and orthotopic mouse model from SGC organoids retain their original histological features through passages. Next, we evaluated whether our SGC organoids and PDXs could recapitulate the histological characteristics of the original tumor. Most SGCs are usually well-differentiated tumors, resulting in difficult diagnosis with only a specific histological marker. Thus, it is necessary for us to look at a wide range of histological images to ensure an accurate diagnosis[11]. Since our *in vitro* organoids did not show sufficient histological structure, we first established an orthotopic animal model from our human tumor-derived and PDX-derived organoids, as described previously[23], followed by histological analysis of orthotopic xenografting tumors. We confirmed palpable tumor formation 2–4 weeks after the transplantation (Fig. 1b), which required approximately six months to reach 1-cm tumor diameter.

Histologically, PDXs and orthotopic xenografting tumors from human tumor-derived organoids or PDX-derived organoids showed similar morphology to the originating SGC tumor, as confirmed by independent pathologists (Fig. 3 and Supplementary Fig. S2a–g). Highly differentiated structural characteristics of histological subtypes, such as ductal lesions and cribriform structure with comedonecrosis in SDC (YCU-SDC-14 and YCU-SDC-20) and cystic structures lined by mucous cells and clear cells in MEC (YCU-MEC-24), were present in both PDXs and orthotopic xenografting tumors, as observed in the matched patient sample. Additionally, we observed that results of immunohistochemistry (IHC) for CK as an epithelial marker and p63 as a myoepithelial marker showed features similar to those in matched patient sample. Furthermore, PDXs and orthotopic xenografting tumors from human SGC-derived organoids or PDX-derived organoids retained the overexpressed human epidermal growth factor receptor 2 (HER2), which is frequently seen and is a possible potential therapeutic target in SDC. The expression of androgen receptor (AR) in the original tumor of YCU-SDC-14 was not retained with passaging in PDXs and orthotopic xenografting tumors from organoids. AR and GCDFP15 expression in the original tumor of YCU-SDC-20 was not confirmed for PDXs and orthotopic xenografting tumors from human tumor-derived organoid; however, their expressions were retained in orthotopic xenografting tumors from PDX-derived organoid. Overall, we confirmed that our all established organoids had the potential to generate orthotopic xenograft tumors and that these organoids and PDXs recapitulated the histological characteristics of the original tumor.

Transcription profiles of PDXs, human tumor-derived organoids and PDX-derived organoids of SGC. All established PDXs or organoids were then comprehensively genetically characterized on the basis of their

transcription profiles determined using RNA-seq analysis, while the original tumors were not used due to lack of tissue. To account for the possibility of murine stromal cells contamination in PDX or PDX-derived organoids, we performed bioinformatics analysis to distinguish between human and mouse-derived reads before estimating gene expression levels (Supplementary Fig. S4), and only human-derived reads were used for analyzing the transcription profiles.

When heatmaps were obtained based on the estimated gene expression levels, each model was hierarchically clustered according to the patient origin and histological subtype (Fig. 4a). Furthermore, these results were combined with gene expression levels of 180 cases of SGC, including multiple histological types obtained from public databases, which confirmed that our PDXs or organoids clearly classified each SGC histology (Fig. 4b). Correlation coefficients were then calculated between models having the same origin to quantify the similarity of these expression profiles. As shown in Fig. 4c, the gene expression levels across models having the same origin were highly correlated with mean Pearson correlation of 0.834, PDXs vs. human tumor-derived organoids; mean Pearson correlation of 0.871, PDXs vs. PDX-derived organoids; and mean Pearson correlation of 0.851, human tumor-derived organoids vs. PDX-derived organoids.

Next, we explored the presence of fusion genes using RNA-seq data. In addition to the previously reported *MYBL1-NFIB* gene in YCU-ACC-4, the frequently reported fusion gene *CRCT1-MAML2* was detected *in silico* in all PDXs, human tumor-derived organoids, and PDX-derived organoids of YCU-MEC-24. Moreover, its presence was reconfirmed using RT-PCR and Sanger sequencing (Supplementary Fig. S3a, b).

Genomic variation in PDXs, human tumor-derived organods, and PDX-derived organoids of SGC. Since the present study did not have access to sufficient primary tumor tissues or patient blood samples for genome sequencing, we performed a limited analysis of genomic variation in the established models using RNA-seq data. The SNV and indel output according to GATK[24] Best Practice (https://software.broadinstitute.org/gatk/best-practices/) were filtered by the COSMIC database[25] (https://cancer.sanger.ac.uk/cosmic). All extracted mutations are listed in Supplementary Table S2. Among these results, the representative genomic mutations frequently found in SGCs are also shown in Fig. 5. *TP53* mutation, frequently observed in SGC[14], was detected in all samples other than those derived from YCU-SDC-14. In contrast, *PIK3CA* mutation, which has been reported in SDC and ACC[14], was not detected in our series.

In vitro **drug sensitivity assay using human tumor-derived and PDX-derived organoids of SGCs.** Finally, we investigated whether our established models could be used for drug screening. For this assay, cytotoxic agents (that are clinically used for patients diagnosed with SGCs) or molecularly targeted agents (if tumor express some protein that can be targeted) were evaluated. Since the growth of both PDXs and orthotopic xenografting tumors of organoids established in this study were too slow to be ideal for drug sensitivity assay *in vivo*, we subjected human tumor-derived and PDX-derived organoids to this assay *in vitro*. While the YCU-MEC-24 was excluded due to growth arrest, which resulted in insufficient cells for this assay, all other available human tumor-derived and PDX-derived organoids were tested using cisplatin, 5-fluorouracil (5-FU), and docetaxel. Since the clinical efficacy of anti-HER2 humanized monoclonal antibody trastuzumab combined with docetaxel was shown in patients with HER2-positive SDCs in a phase II trial [26], anti-tumor effect of trastuzumab was also examined in human tumor-derived and PDX-derived organoids of SDC (YCU-SDC-14/14X, YCU-SDC-20/20X and YCU-SDC-32) expressing HER2. As shown in Fig. 6, cisplatin, 5-FU, and docetaxel demonstrated dose-dependent inhibition of cell proliferation against all human tumor-derived and PDX-derived organoids with the varied range of IC_{50}, whereas

trastuzumab did not show any anti-proliferation effect on these organoids. These results suggest that our human tumor-derived and PDX-derived organoid models can be used for pre-clinical pharmacogenomic studies for SGCs.

Discussion

This study is the first to report the generation of comprehensive preclinical models of multiple SGC histological subtypes using our previously established novel approach for organoid culture and PDX[23]. We confirmed histological as well as genetic homology and reproducibility of our all PDXs, human tumor-derived organoids, and PDX-derived organoids of SGC established in this study. Additionally, we demonstrated that both human tumor-derived and PDX-derived organoids of multiple SGC histological subtypes were useful for drug sensitivity examination *in vitro*. Thus, we developed the framework of comprehensive preclinical models of SGCs using organoid culture and PDX techniques, which could serve as an *in vitro* and *in vivo* model both for elucidating the pathogenesis of SGC and for future pre-clinical drug development.

To date, there are several previous reports on the establishment of cell lines for SGC[27–35]. In terms of SDC cell line, MDA-SDC-04 is the only SDC cell line established using a 2-dimensional culture reported until now[31], while Li et al. reported that the line requires an immortalization process and loses chromosomal aberrations by long-term passaging without any tumor-forming potential in xenografts. Thus, it is difficult to establish SGC cell lines using traditional 2-dimensional culture that reproduces the original tumor characteristics. Our study is the first to report the establishment of PDXs and organoids generated from human SDC tumors with histological reproducibility of the original SDC tumor by orthotopic transplantation of SDC organoids, with its genetic homology and reproducibility confirmed using RNA-seq.

Furthermore, we showed that our previously optimized approach for the generation of human ACC-derived organoids and PDXs can be also adapted to establish *in vitro* and *in vivo* SGC models of multiple histological subtypes. While most of the previous literatures reporting the establishment of SGC cell lines were based on only a single histological subtype of SGC, our method allowed various histological subtypes of SGCs for the culture. Our results are consistent with previous observations that organoid culture can be applied to a number of malignancies and has been regarded as a novel culture approach that preserves more of the original tumor characteristics than the traditional 2-dimension culture technique. Thus, our approach to generate these novel pre-clinical models of PDXs and organoids enable the establishment of *in vitro* and *in vivo* preclinical models of SGC, which has been considered difficult to generate in the past due to its scarcity and slow-growing characteristics. This suggests that this novel approach has potential to be applied to more cancer research, including other malignancies in which the establishment of cell lines has been considered difficult. Additionally, we revealed that PDX tumor could derive organoid lines that were homologous to human tumor-derived organoids for SDC and MEC, as we previously presented the usability of PDX-derived organoids of ACC in our study. Particularly, our PDX-derived organoids of SDC showed similar aspects of gross cyst formation and histological properties of the orthotopically implanted tumors with similarities in gene expression. These results are also consistent with previously reported methods for PDX-derived organoids of pediatric liver cancer[36] and non-small lung cancer[37].

In SGC research, the growth of some tissue types develop very slowly; therefore, the number of cells obtained from the culture process of a single line is limited. As human tumor-derived organoid of YCU-MEC-24 was not available

for drug sensitivity evaluation due to terminated growth during passage, the number of cells obtained from human-derived organoids alone might be insufficient to use continuously for a variety of studies from both practical and cost perspectives. The use of PDX-derived organoids is thought to be an alternative method that can overcome this issue concerning the culture of slow-growing cancers since we confirmed that PDX was capable of multiple passages, up to a maximum of approximately eight times, while securing tumor volume as well as maintaining the model without loss.

In contrast, PDX always potentially contains mouse mesenchymal cells[20]; hence, PDX-derived organoid cultures always carry the risk of mouse cell contamination. In fact, PDX-derived organoid of YCU-SDC-20 contained a relatively large number of mouse-derived reads according to the bioinformatics analysis, and the PCR for mouse-derived mitochondrial DNA sequences was positive (Supplementary Fig. S5), suggesting that PDX-derived organoid of YCU-SDC-20 possibly contained some mouse cells. While we did not observe any significant differences in tumorigenic, histological, and genetic profiles by orthotopic transplantation or drug efficacy between our pre-clinical models in the present study, these results may be affected by the proportion of mouse cells. Therefore, it is necessary to always consider the risk of contamination when conducting research using PDX-related approach.

Another limitation of the present study is that our model did not fully reflect the highly differentiated and heterogeneous nature of SGC. First, we observed small differences in protein expression patterns in IHC of PDX and orthotopic xenografts using transplanted organoids. Although the primary tumor of YCU-SDC-14 was partially positive for AR, all our PDXs, human tumor-derived organoids, and PDX-derived organoids of YCU-SDC-14 were AR negative in this study. This might be due to the tumor heterogeneity[38,39]. For example, we observed that the transcription profiles of YCU-SDC-20 and YCU-SDC-20 PDX/YCU-SDC-20X obtained using RNA-seq analysis did not correlate well, while those of YCU-SDC-20 PDX and YCU-SDC-20X correlated very well. In the case of YCU-SDC-20 with AR positive primary tumor, PDXs and human-derived organoids of YCU-SDC-20 were AR negative, whereas PDX-derived tumor were somehow AR positive. Prostate cancers treated with androgen deprivation therapy can regain AR expression through various mechanisms — often leading to treatment resistance for these diseases[40], suggesting that similar changes might occur in our YCU-SDC-20 series. Thus, there is always the possibility that cancer cells may evolve and selectively change their properties from those observed in the original tumor through model establishment and its passaging[41]. When comparing the heterogeneity of SGCs of primary tumor and of our pre-clinical models, a major limitation of the current study is that we did not directly compare the reproducibility of gene expressions using RNA-seq or gene mutations using genome sequencing because we did not collect a sufficient amount of the primary patient tumor or other patient samples such as blood; therefore, the retention of gene expression or mutations through model establishment and its passaging was not explored in detail.

Despite these limitations, our results present the significance of SGC related organoids in a variety of histological types as a drug efficacy evaluation system, may be a milestone in the future development of novel therapy for patients diagnosed with SGCs. While the lack of *in vitro* and *in vivo* SGC models that recapitulate the diversity of human SGC has hampered the progress in understanding disease pathogenesis and therapy response until recently, our approach could be a powerful resource for pre-clinical SGC pharmacogenomic studies for overcoming these situations.

In conclusion, we newly generated PDXs and human tumor-derived organoids as *in vitro* and *in vivo* preclinical models of SDC, MEC, and MYEC, in addition to ACC. Additionally, we show that PDX tumors could be used to derive organoids in SDC and MEC. We confirmed that our established PDXs and human tumor-derived and PDX-derived organoids retain their original histological and genetical features of corresponding histological subtypes through passaging. Lastly, we demonstrated that our SGC organoid cells are amenable for pharmacologic studies. The framework of our developed organoids and PDX-related SGC models shows potential application in preclinical studies for the development of novel treatment modalities for patients diagnosed with rare cancers, including SGC, and may be a useful tool for elucidating the pathogenesis of these diseases.

Declarations

Data availability

The RNA sequencing data that support the findings of this study have been deposited in the DNA Data Bank of Japan Sequence Read Archive (DRA) under the accession number DRA011243. All data supporting the findings of the study are available within the Article, Supplementary Information or available from the corresponding author upon request.

Acknowledgements

This work was supported by 19K09895 (PI: D.S.), 19K09873 (PI: H.T.), 21K09636 (PI: G.N.) and 21K09612 (PI: N.O.) from Japan Society for the Promotion of Science, Yokohama City University Hospital advanced medical treatment supporting system (approval No. 2019-112), the grant for 2019–2020 Strategic Research Promotion (No. SK2803) of Yokohama City University, and fund (11800122) for Creation of Innovation Centers for Advanced Interdisciplinary Research Areas Program in the Project for Developing Innovation Systems from the Ministry of Education, Culture, Sports, Science and Technology (MEXT) of Japan (H.T.).

Author contributions

D.S. and N.O. designed and supervised the study. J.R., S.F., Y.S., and H.T. supervised the study. D.S. and Y.A. wrote the manuscript. D.S., H.H., T.H., H.T., G.N., and N.O. supervised the sample collection and contributed to the interpretation of clinical information. Y.A., K.T., R.O., Y.U., and H.T. developed methodologies. Y.A., K.T., J.A., M.S., Y.K., R.O., Y.U., Y.N., and Y.I. performed the related experiments. Y.A., K.T., J.A., D.S., M.S., Y.K., J.R., and Y.S. contributed to the data analysis. K.T., D.S., H.H., T.H., H.T., and G.N. collected the clinical information. Y.A., K.T., S.Y., Y.I., and S.F. performed the pathological examination. All of the authors have read and approved the manuscript.

Competing interests

The authors declare no competing interests.

References

1. Carvalho, A. L., Nishimoto, I. N., Califano, J. A. & Kowalski, L. P. Trends in incidence and prognosis for head and neck cancer in the United States: A site-specific analysis of the SEER database. *Int. J. Cancer* **114**, 806–

816 (2005).

2. Parkin D. M., Whelan S. L., Ferlay J., Teppo L., Thomas, D. B., eds. Cancer incidence in five continents. Volume VIII. *IARC Sci. Publ.* No. 155, (2002).
3. Thompson, L. D. R. World health organization classification of tumours: Pathology and genetics of head and neck tumours. *Ear, Nose Throat J.* **85**, 74 (2006).
4. Griffith, C. C., Schmitt, A. C., Little, J. L. & Magliocca, K. R. New developments in salivary gland pathology: Clinically useful ancillary testing and new potentially targetable molecular alterations. *Arch. Pathol. Lab. Med.* **141**, 381–395 (2017).
5. Zhu, S., Schuerch, C. & Hunt, J. Review and updates of immunohistochemistry in selected salivary gland and head and neck tumors. *Arch. Pathol. Lab. Med.* **139**, 55–66 (2015).
6. Postema, R. J., Van Velthuysen, M. L. F., Van Den Brekel, M. W. M., Balm, A. J. M. & Peterse, J. L. Accuracy of fine-needle aspiration cytology of salivary gland lesions in The Netherlands cancer institute. *Head Neck* **26**, 418–424 (2004).
7. Boon, E. *et al.* A clinicopathological study and prognostic factor analysis of 177 salivary duct carcinoma patients from The Netherlands. *Int. J. Cancer* **143**, 758–766 (2018).
8. Gilbert, M. R. *et al.* A 20-year review of 75 cases of salivary duct carcinoma. *JAMA Otolaryngol. - Head Neck Surg.* **142**, 489–495 (2016).
9. Sur, R. K. *et al.* Adenoid cystic carcinoma of the salivary glands: A review of 10 years. *Laryngoscope* **107**, 1276–1280 (1997).
10. Van Weert, S. *et al.* Adenoid cystic carcinoma of the head and neck: A single-center analysis of 105 consecutive cases over a 30-year period. *Oral Oncol.* **49**, 824–829 (2013).
11. Ali, S. *et al.* Cause-specific mortality in patients with mucoepidermoid carcinoma of the major salivary glands. *Ann. Surg. Oncol.* **20**, 2396–2404 (2013).
12. Chen, A. M., Lau, V. H., Farwell, D. G., Luu, Q. & Donald, P. J. Mucoepidermoid carcinoma of the parotid gland treated by surgery and postoperative radiation therapy: Clinicopathologic correlates of outcome. *Laryngoscope* vol. 123 3049–3055 (2013).
13. Guzzo, M., Andreola, S., Sirizzotti, G. & Cantu, G. Mucoepidermoid carcinoma of the salivary glands: Clinicopathologic review of 108 patients treated at the National Cancer Institute of Milan. *Ann. Surg. Oncol.* **9**, 688–695 (2002).
14. Stenman, G., Persson, F. & Andersson, M. K. Diagnostic and therapeutic implications of new molecular biomarkers in salivary gland cancers. *Oral Oncology* vol. 50 683–690 (2014).
15. Stenman, G. Fusion Oncogenes in Salivary Gland Tumors: Molecular and Clinical Consequences. *Head Neck Pathol.* **7**, 12–19 (2013).
16. Nordkvist, A., Gustafsson, H., Juberg-Ode, M. & Stenman, G. Recurrent rearrangements of 11q14-22 in mucoepidermoid carcinoma. *Cancer Genet. Cytogenet.* **74**, 77–83 (1994).
17. Persson, M. *et al.* Recurrent fusion of MYB and NFIB transcription factor genes in carcinomas of the breast and head and neck. *Proc. Natl. Acad. Sci.* **106**, 18740–18744 (2009).
18. Sachs, N. & Clevers, H. Organoid cultures for the analysis of cancer phenotypes. *Curr. Opin. Genet. Dev.* **24**, 68–73 (2014).

19. Weeber, F., Ooft, S. N., Dijkstra, K. K. & Voest, E. E. Tumor Organoids as a Pre-clinical Cancer Model for Drug Discovery. *Cell Chem. Biol.* **24**, 1092–1100 (2017).
20. Hidalgo, M. *et al.* Patient-derived Xenograft models: An emerging platform for translational cancer research. *Cancer Discov.* **4**, 998–1013 (2014).
21. Pauli, C. *et al.* Personalized in vitro and in vivo cancer models to guide precision medicine. *Cancer Discov.* **7**, 462–477 (2017).
22. Kondo, J. & Inoue, M. Application of Cancer Organoid Model for Drug Screening and Personalized Therapy. *Cells* **8**, 470 (2019).
23. Takada, K. *et al.* Establishment of PDX-derived salivary adenoid cystic carcinoma cell lines using organoid culture method. *Int. J. Cancer* **148**, 193–202 (2021).
24. McKenna, A. *et al.* The genome analysis toolkit: A MapReduce framework for analyzing next-generation DNA sequencing data. *Genome Res.* **20**, 1297–1303 (2010).
25. Forbes, S. A. *et al.* COSMIC: Exploring the world's knowledge of somatic mutations in human cancer. *Nucleic Acids Res.* **43**, D805–D811 (2015).
26. Takahashi, H. *et al.* Phase II trial of trastuzumab and docetaxel in patients with human epidermal growth factor receptor 2-positive salivary duct carcinoma. *J. Clin. Oncol.* **37**, 125–134 (2019).
27. Jiang, Y. *et al.* MYB-activated models for testing therapeutic agents in adenoid cystic carcinoma. *Oral Oncol.* **98**, 147–155 (2019).
28. Warner, K. A. *et al.* UM-HACC-2A: MYB-NFIB fusion-positive human adenoid cystic carcinoma cell line. *Oral Oncol.* **87**, 21–28 (2018).
29. Tanaka, N., Urabe, K., Hashitani, S., Sakurai, K. & Urade, M. Establishment and characterization of a human adenoid cystic carcinoma cell line forming colonies cultured in collagen gel and transplantable in nude mice. *Oncol. Rep.* **17**, 335–340 (2007).
30. Queimado, L. *et al.* In vitro transformation of cell lines from human salivary gland tumors. *Int. J. Cancer* **81**, 793–798 (1999).
31. Li, J. *et al.* Establishment and Genomic Characterization of Primary Salivary Duct Carcinoma Cell Line. *Oral Oncol.* **69**, 108 (2017).
32. Alamri, A. M. *et al.* Expanding primary cells from mucoepidermoid and other salivary gland neoplasms for genetic and chemosensitivity testing. *DMM Dis. Model. Mech.* **11**, (2018).
33. Warner, K. A. *et al.* Characterization of tumorigenic cell lines from the recurrence and lymph node metastasis of a human salivary mucoepidermoid carcinoma. *Oral Oncol.* **49**, 1059–1066 (2013).
34. Rao, P. H., Murty, V. V. V. S., Louie, D. C. & Chaganti, R. S. K. Nonsyntenic amplification of MYC with CDK4 and MDM2 in a malignant mixed tumor of salivary gland. *Cancer Genet. Cytogenet.* **105**, 160–163 (1998).
35. Grénman, R. *et al.* UT-MUC-1, a New Mucoepidermoid Carcinoma Cell Line, and Its Radiosensitivity. *Arch. Otolaryngol. Neck Surg.* **118**, 542–547 (1992).
36. Bissig-Choisat, B. *et al.* Novel patient-derived xenograft and cell line models for therapeutic testing of pediatric liver cancer. *J. Hepatol.* **65**, 325–333 (2016).
37. Shi, R. *et al.* Organoid cultures as preclinical models of non-small cell lung cancer. *Clin. Cancer Res.* **26**, 1162–1174 (2020).

38. Dagogo-Jack, I. & Shaw, A. T. Tumour heterogeneity and resistance to cancer therapies. *Nature Reviews Clinical Oncology* vol. 15 81–94 (2018).
39. McGranahan, N. & Swanton, C. Clonal Heterogeneity and Tumor Evolution: Past, Present, and the Future. *Cell* vol. 168 613–628 (2017).
40. Wadosky, K. M. & Koochekpour, S. Molecular mechanisms underlying resistance to androgen deprivation therapy in prostate cancer. *Oncotarget* vol. 7 64447–64470 (2016).
41. Pearson, A. T. *et al.* Patient-derived xenograft (PDX) tumors increase growth rate with time. *Oncotarget* **7**, 7993–8005 (2016).
42. Ono, K. *et al.* Species identification of animal cells by nested PCR targeted to mitochondrial DNA. *Vitr. Cell. Dev. Biol. - Anim.* **43**, 168–175 (2007).
43. Chen, S., Zhou, Y., Chen, Y. & Gu, J. Fastp: An ultra-fast all-in-one FASTQ preprocessor. *Bioinformatics* **34**, i884–i890 (2018).
44. Conway, T. *et al.* Xenome-a tool for classifying reads from xenograft samples. *Bioinformatics* **28**, 172–178 (2012).
45. Dobin, A. *et al.* STAR: Ultrafast universal RNA-seq aligner. *Bioinformatics* **29**, 15–21 (2013).
46. Liao, Y., Smyth, G. K. & Shi, W. FeatureCounts: An efficient general purpose program for assigning sequence reads to genomic features. *Bioinformatics* **30**, 923–930 (2014).
47. Robinson, M. D., McCarthy, D. J. & Smyth, G. K. edgeR: A Bioconductor package for differential expression analysis of digital gene expression data. *Bioinformatics* **26**, 139–140 (2009).
48. Leek, J. T., Johnson, W. E., Parker, H. S., Jaffe, A. E. & Storey, J. D. The SVA package for removing batch effects and other unwanted variation in high-throughput experiments. *Bioinformatics* **28**, 882–883 (2012).
49. Cingolani, P. *et al.* A program for annotating and predicting the effects of single nucleotide polymorphisms, SnpEff SNPs in the genome of Drosophila melanogaster strain w 1118; iso-2; iso-3. (2012) doi:10.4161/fly.19695.
50. Wang, K., Li, M. & Hakonarson, H. ANNOVAR: functional annotation of genetic variants from high-throughput sequencing data. doi:10.1093/nar/gkq603.
51. Skidmore, Z. L. *et al.* GenVisR: Genomic Visualizations in R. *Bioinformatics* **32**, 3012–3014 (2016).
52. Nicorici, D. *et al.* FusionCatcher - a tool for finding somatic fusion genes in paired-end RNA-sequencing data. *bioRxiv* 011650 (2014) doi:10.1101/011650.
53. Pimentel, H., Bray, N. L., Puente, S., Melsted, P. & Pachter, L. Differential analysis of RNA-seq incorporating quantification uncertainty. *Nat. Methods* **14**, 687–690 (2017).
54. Melsted, P. *et al.* pizzly: Fusion detection and quantification by pseudoalignment. *bioRxiv* (2017) doi:10.1101/166322.
55. Jang, Y. E. *et al.* ChimerDB 4.0: An updated and expanded database of fusion genes. *Nucleic Acids Res.* **48**, D817–D824 (2020).
56. Ritz, C. & Streibig, J. C. Bioassay analysis using R. *J. Stat. Softw.* **12**, 1–22 (2005).

Figures

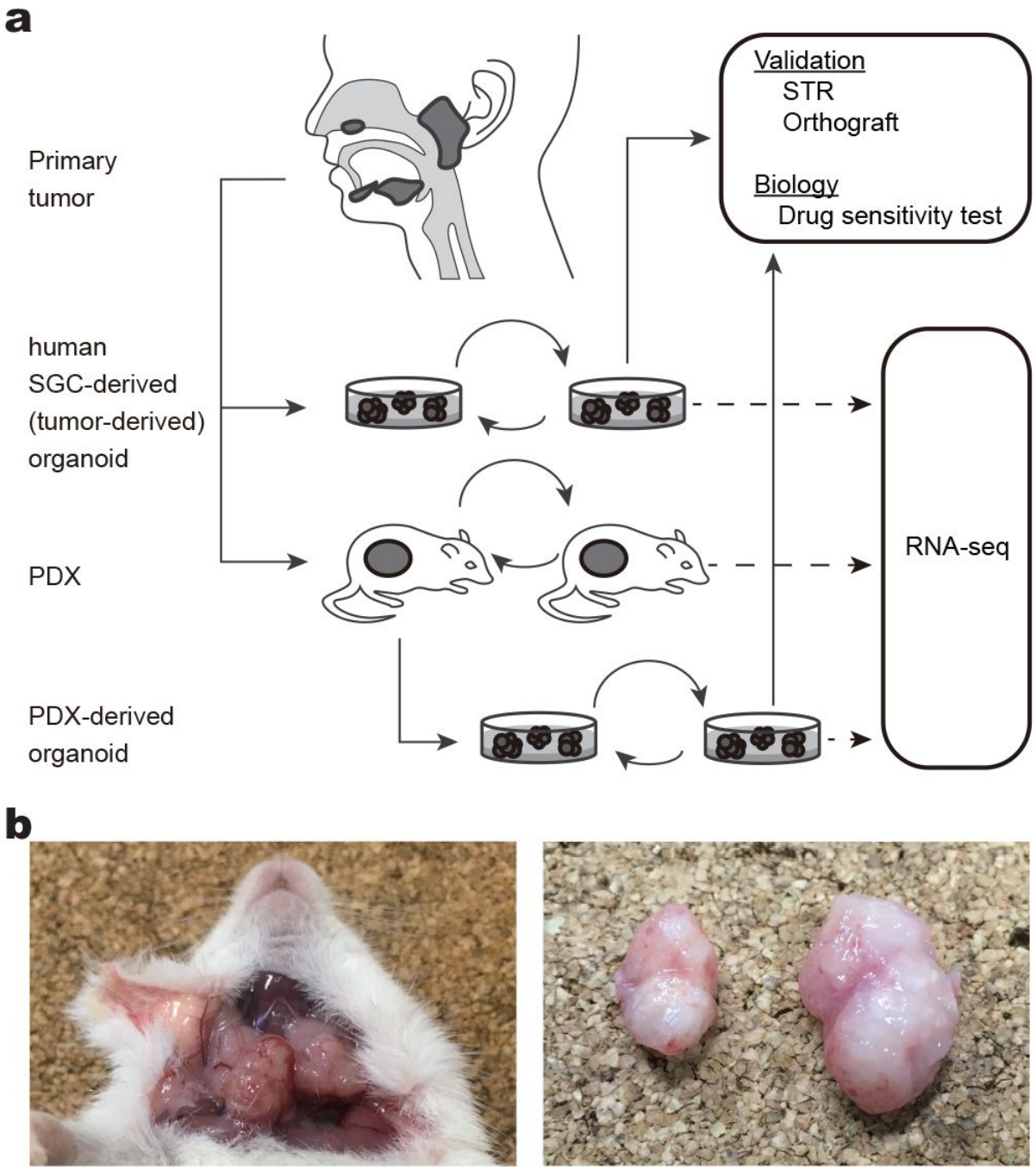

Figure 1

Establishment of salivary gland carcinoma (SGC) patient-derived xenografts (PDXs), organoids, and orthotopic xenografts. a Overview of the experiment. The patient specimens were divided into PDX and/or organoid cultures. When PDX was successfully established, we attempted to culture the PDX-derived organoids. RNA-seq was performed on all established PDXs, human tumor-derived organoids, and PDX-derived organoids, but could not be performed on the patient's primary tumor due to insufficient sample volume. b Representative orthotopic xenograft formed in the submandibular gland of a mouse. A PDX-derived organoid from salivary duct carcinoma (YCU-SDC-20X) was transplanted into the left and right submandibular glands of the mouse and formed the tumor respectively.

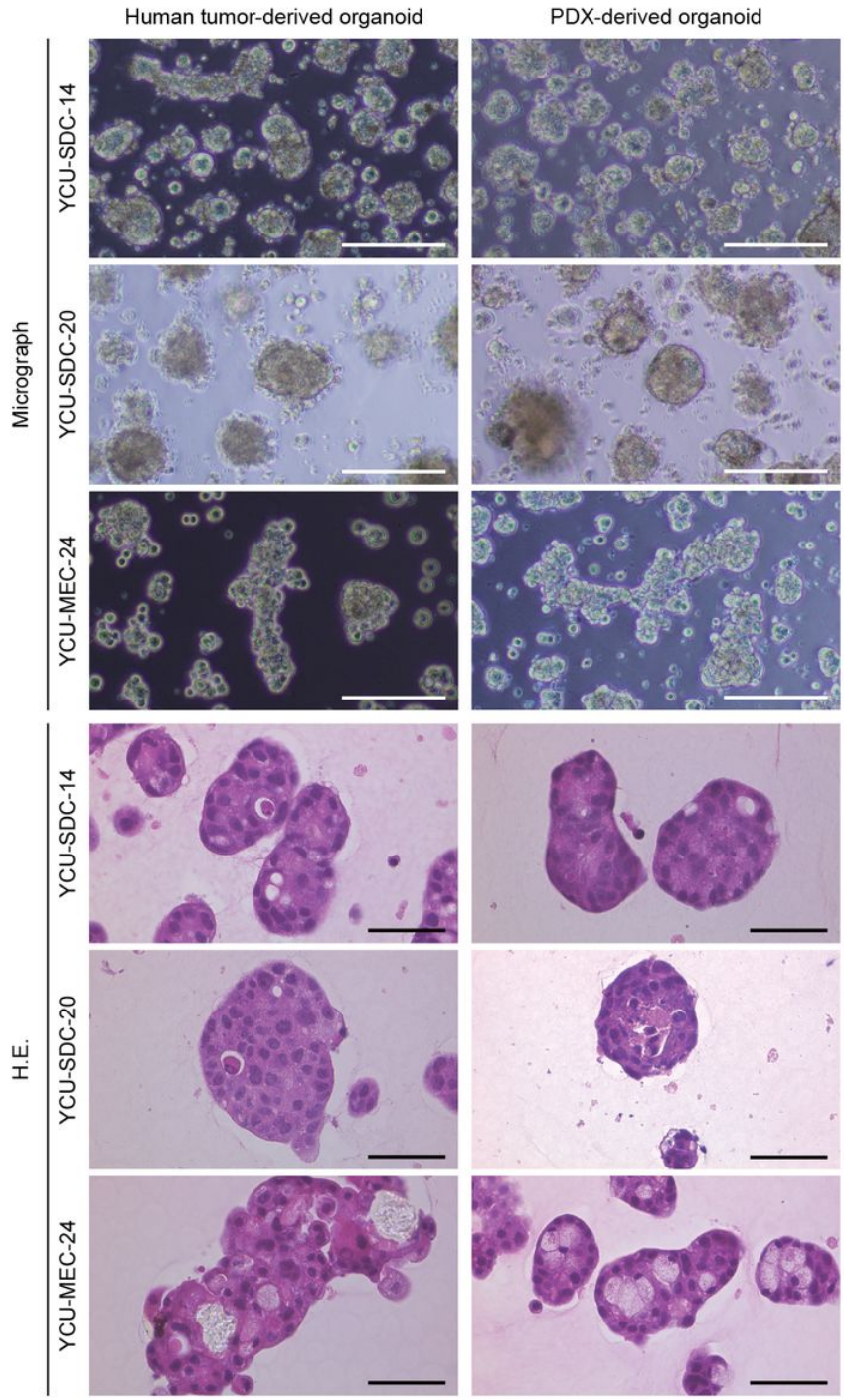

Figure 2

Bright-field images and hematoxylin and eosin (H&E) staining of salivary gland carcinoma (SGC) organoids. The left column shows the human tumor-derived organoids, and the right column shows the patient-derived xenograft (PDX)-derived organoids. The human tumor-derived organoid and PDX-derived organoid derived from salivary duct carcinoma (YCU-SDC-14 series, YCU-SDC-20 series) both showed a cyst-like structure with necrosis inside. Those from mucoepidermoid carcinoma (YCU-MEC-24 series) both showed grape-like structures and glandular tuft formation. Scale bars represent 50 μm for bright-field images and 20 μm for H&E staining. See Supplementary Fig. S1. for another salivary duct carcinoma organoid (YCU-SDC-32).

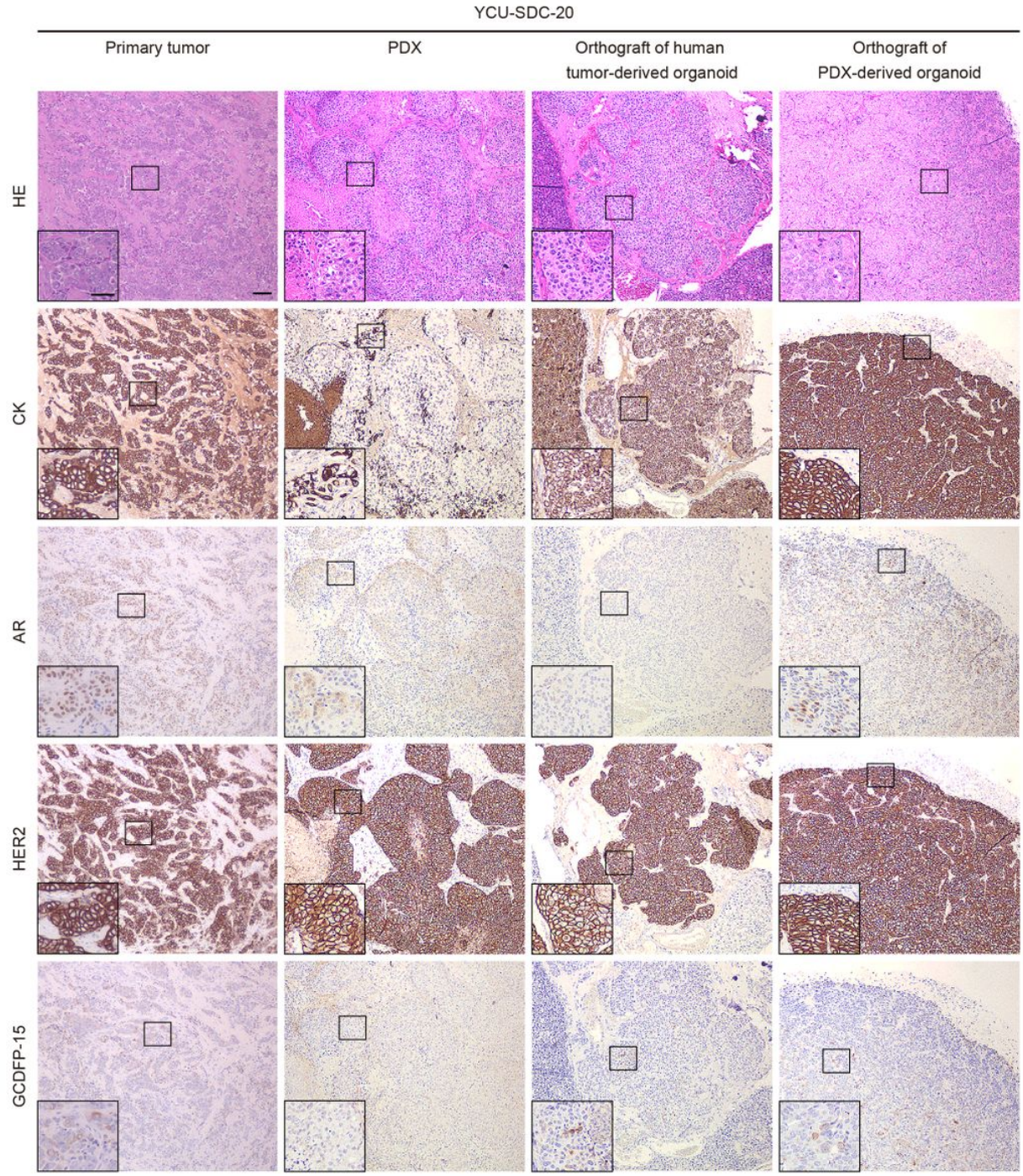

Figure 3

Histology and IHC staining Hematoxylin and eosin (H&E) staining and IHC (CK, AR, HER2, GCDFP-15) of the patient's primary tumor, patient-derived xenograft (PDX), orthotopic xenograft of human tumor-derived organoid, and orthotopic xenograft of PDX-derived organoid. A case of salivary duct carcinoma (YCU-SDC-20 series) is presented as a representative. For other cases, see Supplementary Fig. S1a-g. Scale bars in a large frame represent 10 microns, and those in a small frame represent 5 microns.

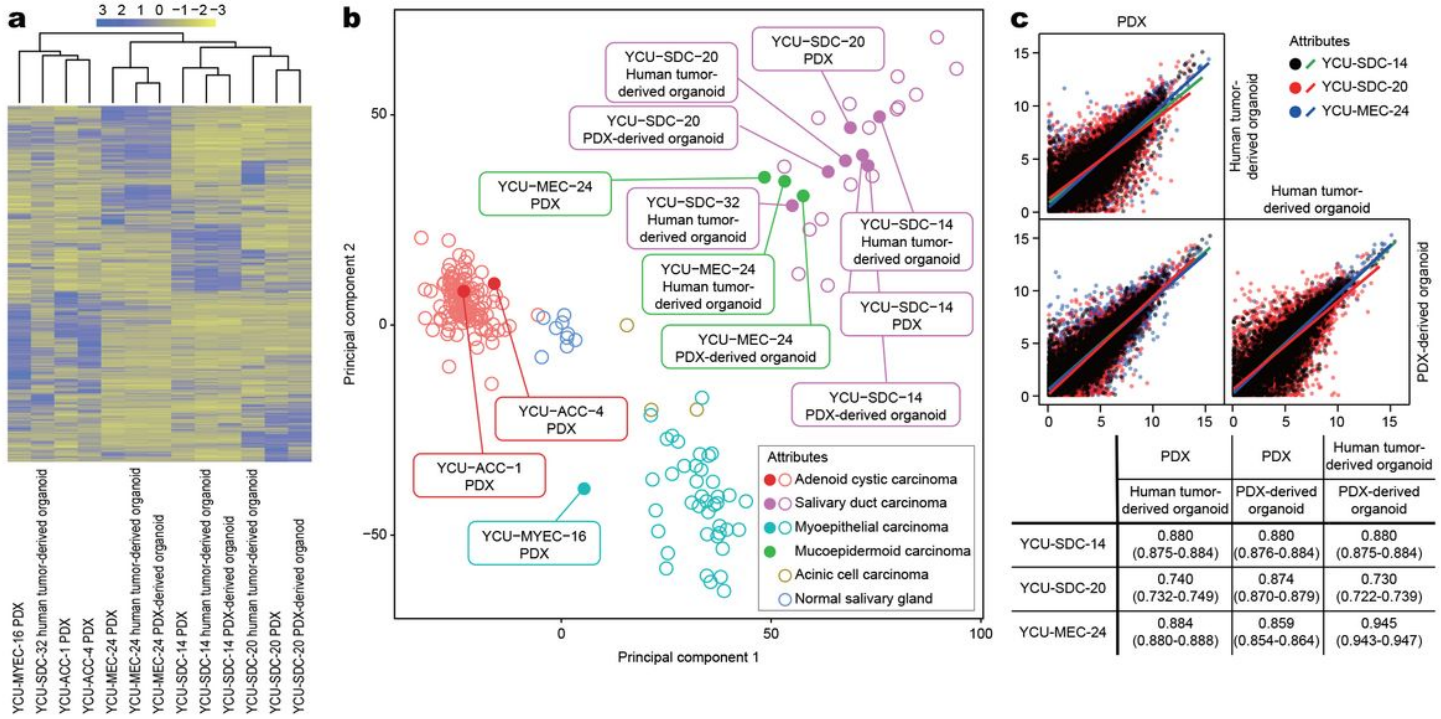

	PDX / Human tumor-derived organoid	PDX / PDX-derived organoid	Human tumor-derived organoid / PDX-derived organoid
YCU-SDC-14	0.880 (0.875-0.884)	0.880 (0.876-0.884)	0.880 (0.875-0.884)
YCU-SDC-20	0.740 (0.732-0.749)	0.874 (0.870-0.879)	0.730 (0.722-0.739)
YCU-MEC-24	0.884 (0.880-0.888)	0.859 (0.854-0.864)	0.945 (0.943-0.947)

Figure 4

Gene expression analysis a Heatmap. The heatmap shows the top 3000 variability genes for patient-derived xenografts (PDXs) and organoids. b PCA plot. The filled circles indicate the established PDX and organoid samples. Blank circles indicate gene expression data for salivary gland carcinoma (SGC) with multiple histological subtypes or normal parotid tissue downloaded from public databases. All data were corrected for batch effects based on the tissue type. c correlation matrix. Scatter plots of gene expression levels for each experimental model were plotted for patient samples in which the human tumor-derived organoids, PDX, and PDX-derived organoids were established (YCU-SDC-14, YCU-SDC-20, and YCU-MEC-24). The Pearson correlation coefficient and 95% confidence interval are shown in the table below.

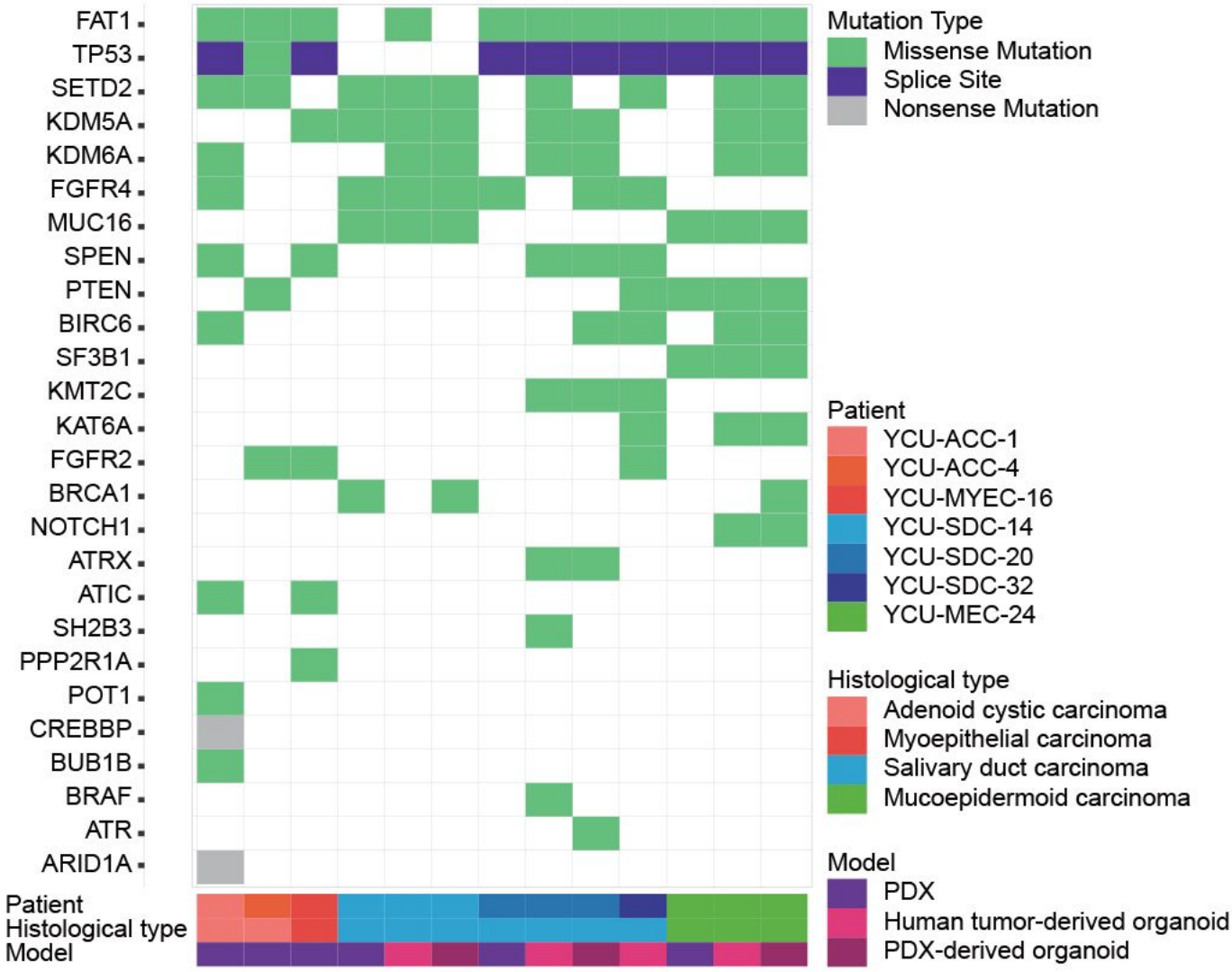

Figure 5

Gene mutation/variant analysis Genetic variants detected in the RNA-seq data of each established model Genetic variants were annotated, and typical possible effects on genes are shown. See Supplementary Table S2 for a list of all genetic variants.

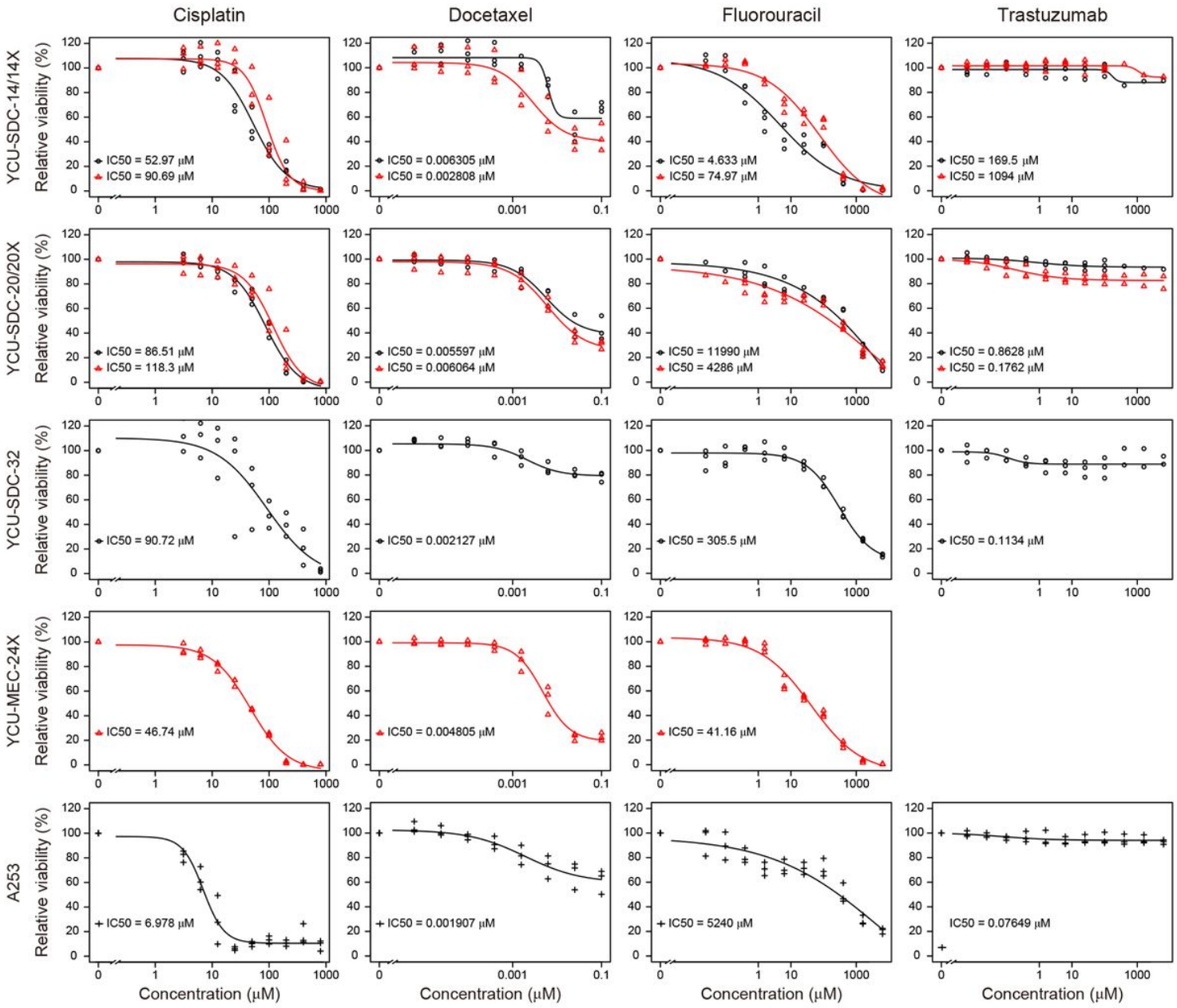

Figure 6

Drug sensitivity test Organoids were subjected to the chemotherapy drugs cisplatin, docetaxel, fluorouracil, and trastuzumab. Cell viability was plotted as a percentage of untreated organoids. Black circles indicate human tumor-derived organoids in each series. Red triangles indicate PDX-derived organoids in each series. Black crosses indicate A253 cell line.

Supplementary Files

This is a list of supplementary files associated with this preprint. Click to download.

- Supplementaryinfo20210803.docx
- SupplementaryTableS2Valiantlist.xlsx